



UNIVERSITY OF LEEDS

This is a repository copy of *Synthesis of calcium monouranate particles via an aqueous route*.

White Rose Research Online URL for this paper:  
<http://eprints.whiterose.ac.uk/102564/>

Version: Accepted Version

---

**Proceedings Paper:**

Ding, W [orcid.org/0000-0003-3002-5068](http://orcid.org/0000-0003-3002-5068), Botha, JA, Hanson, BC  
[orcid.org/0000-0002-1720-1656](http://orcid.org/0000-0002-1720-1656) et al. (1 more author) (2017) Synthesis of calcium monouranate particles via an aqueous route. In: MRS Advances. Scientific Basis for Nuclear Waste Management, 02-06 Nov 2015, Montpellier, France. Cambridge Core , pp. 4123-4129.

<https://doi.org/10.1557/adv.2017.199>

---

© Materials Research Society 2017. This is an author produced version of a paper published in a revised form in MRS Advances, Vol. 1, Issue 62 (2016), pp. 4123-4129, DOI: <https://doi.org/10.1557/adv.2017.199>, published by Materials Research Society and Cambridge University Press.

**Reuse**

Unless indicated otherwise, fulltext items are protected by copyright with all rights reserved. The copyright exception in section 29 of the Copyright, Designs and Patents Act 1988 allows the making of a single copy solely for the purpose of non-commercial research or private study within the limits of fair dealing. The publisher or other rights-holder may allow further reproduction and re-use of this version - refer to the White Rose Research Online record for this item. Where records identify the publisher as the copyright holder, users can verify any specific terms of use on the publisher's website.

**Takedown**

If you consider content in White Rose Research Online to be in breach of UK law, please notify us by emailing [eprints@whiterose.ac.uk](mailto:eprints@whiterose.ac.uk) including the URL of the record and the reason for the withdrawal request.



[eprints@whiterose.ac.uk](mailto:eprints@whiterose.ac.uk)  
<https://eprints.whiterose.ac.uk/>

# Synthesis of Calcium Monouranate Particles via an Aqueous Route

Weixuan Ding<sup>1</sup>, Johannes A. Botha<sup>1</sup>, Ian T. Burke<sup>2</sup>, Bruce C. Hanson<sup>1</sup>

1- Institute of Particle Science and Engineering, School of Chemical and Process Engineering, University of Leeds, Leeds, LS2 9JT, UK

2- School of Earth and Environment, University of Leeds, Leeds, LS2 9JT, UK

## ABSTRACT

Large stores of unstable waste uranic materials such as fluorides or nitrates exist internationally due to legacy civil nuclear enrichment activities. Conversion of these uranic materials to layered metal uranates prior to disposal is possible via aqueous quench - precipitation type reactions. Previous studies<sup>1</sup> have shown facile in-situ formation of geologically persistent and labile uranate colloids<sup>2</sup> under simulated nuclear waste repository conditions, though the effects of local solution metal-uranium ratios on uranate stoichiometry have yet to be covered. This affects our understanding of how key radionuclides present in repository porewaters such as strontium or caesium may be sequestered in these uranate structures.

In this work, we demonstrate a synthesis reaction for calcium monouranate particles via rapid anhydrous curing of a sol-gel. We present some results showing aqueous nucleation of uranate nanoparticles and their phase transformations during thermal curing as well as the effects of solution phase calcium loading on uranate phase purity in the cured particles.

## INTRODUCTION

Natural uranates form in a paragenetic sequence of solubility limiting phases beginning with Uraninite alteration to form layered uranyl oxide hydrates (Schoepite). Migration of Na/K/Ca into the inter-layer binding sites forms latter products in the paragenetic series (Clarkeite, Becquerelite, Na/K-Compreignecite). Both hydrous and anhydrous uranyl oxides form in natural Uraninite deposits, under hydrothermal or anhydrous conditions<sup>3</sup>. Analogously, after placement of U(VI)-rich cementitious wastefoms in the geosphere, dissolution reactions caused by groundwater influx will form hyperalkaline leachates at ~pH13 which are rich in OH<sup>-</sup>, Na/K/Ca, and U(VI)<sup>4</sup>. Polymerisation of uranyl hydroxides will form amorphous colloidal suspensions or precipitates<sup>1</sup>.<sup>2</sup> Ca incorporation during aging of amorphous precipitates forms Clarkeite-like phases that are structurally isomorphous to anhydrous CaUO<sub>4</sub><sup>2</sup>.

Whilst crystalline uranates may become suitable wastefoms for permanent disposal or interim storage of uranic (U(VI)) waste materials, demonstration of their synthesis pathways are generally limited in the literature to ceramic methods. The ease of tuning product [Ca/U] stoichiometry has resulted in laboratory scale synthesis of anhydrous uranates with several calcium/uranium stoichiometries ([Ca/U]) ranging 0.25 → 3<sup>5-9</sup>. However poor mixing between precursor U(VI) salt grains means prolonged grinding and calcination is required.

Sol-gel or co-precipitation are attractive low cost alternatives that typically require mild conditions, have convenient processing steps and allow use of frame-working agents<sup>10</sup>. Alkoxides as precursors that undergo rapid hydrolysis to form nanoparticles or gels<sup>11</sup> are expensive or complex to prepare as well as being heat, moisture and photosensitive. With the exception of titanium and zirconium alkoxides, most transition metal and actinide alkoxides are unavailable commercially.

Uranyl alkoxides may be substituted by inorganic uranyl salts, requiring an additional hydroxylation agent to precipitate U(VI)-hydroxide particles. This route has been utilised during the synthesis of  $\text{UO}_2$ ,  $\text{U}_3\text{O}_8$  and  $\text{UO}_3$  via direct or indirect alkalisation of U(VI)-nitrate solution. The direct route involves addition of ammonium hydroxide to precipitate  $(\text{NH}_4)_2\text{U}_2\text{O}_7$ <sup>12</sup>, whereas the indirect requires thermal decomposition of epoxide or urea solution to precipitate  $\text{UO}_3$  and  $(\text{NH}_4)_2\text{U}_2\text{O}_7$  respectively<sup>13</sup>. Regardless of the alkalisation method, precipitates are often amorphous, requiring calcination at 600°C to crystallise the anhydrous uranium oxides<sup>14</sup>. Sol-gel methods have only been used to explore un-doped uranium oxides, whilst doping has only been formally explored via the aforementioned ceramic or molten salt reactions<sup>15</sup>.

This work in this paper explores a simple, rapid and direct aqueous based route towards calcium uranate particles. It is part of an effort to understand the effect of synthesis conditions on the chemo-physical properties of the uranate formed with potential for integration with current U(VI) waste stabilisation (i.e.  $\text{UF}_6$  deconversion) or for use in thermodynamic/kinetic experiments.

## EXPERIMENTAL DETAILS

**Synthesis:** Precursor solutions were prepared by mixing varying amounts of Ca(II) and U(VI) nitrate stock solutions to give 50ml of 0.01M U(VI) (pH2) at varying molar [Ca/U] stoichiometry. Saturated calcium hydroxide ( $\text{Ca}(\text{OH})_2$ ) or 0.1M tetraethylammonium hydroxide (TEAOH) solution was used to alkalinize the precursors solution via peristaltic pump at 2.23ml/min under vigorous stirring adapting Tanford's method<sup>16</sup>.

**Analyses:** 1ml aliquots were removed from the [Ca/U] = 0.67 reaction and analyzed using dynamic light scattering (DLS) and zeta potential measurements to follow particle growth and particle surface charge respectively. Aliquots were filtered and centrifuged to remove solids and analyzed using UV-Vis spectroscopy to follow U(VI) speciation. A quartz crystal microbalance (QCM) to record changing frequency ( $\Delta F$ ) and resistance ( $\Delta R$ ) shifts allowed in-situ reaction monitoring. At pH12, the precipitates were centrifuged at 14400g (3 minutes) to remove supernatant then washed using propan-2-ol. All solution phase experiments and analyses were carried out under  $\text{N}_2$  atmosphere to reduce the effects of carbonate influx. The dried particles were analyzed using TGA-DSC; XRD; SEM and TEM; and ICP-OES to follow the effects of calcination on weight loss or heat flow properties; crystalline phase changes; particle morphology and crystallinity; and bulk calcium-uranium ratios respectively.

**Geochemical modelling:** Aqueous U(VI) speciation across relevant pH values was calculated using the geochemical modelling software PHREEQC and the ANDRA ThermoChimie database<sup>17</sup> with updated thermodynamic data for uranium<sup>18</sup>. The specific ion-interaction theory (SIT) was used for ionic strength corrections.

## RESULTS AND DISCUSSION

### Particle formation processes

According to thermodynamic U(VI) calculations, the addition of alkalization agent (hydroxide donor) to the precursor solution is expected to consume  $\text{UO}_2^{2+}$  ions (**Figure 1a** red line) in exchange for U(VI)-hydroxides (**Figure 1a** - blue dots). This is observed in UV-Vis spectra of pH2-5 solutions, showing a transition from  $\text{UO}_2^{2+} \rightarrow \text{UO}_2^{2+} + \text{U(VI)-hydroxide} \rightarrow \text{U(VI)-hydroxides}$  dominated solutions (data not included here). With this transition, the absolute absorbance at 414nm ( $A_{414}$ ) for centrifuged solutions ( $\text{UO}_2^{2+} A_{\text{max}}$ )<sup>19</sup> increases rapidly towards

its maximum at pH4.7 (**Figure 1 a** – black boxes) due to the 10 and 49 fold higher molar absorptivity of the U(VI)-hydroxides  $(\text{UO}_2)_2(\text{OH})_2^{2+}$  ( $101 \pm 2 \text{ mol}^{-1} \text{ cm}^{-1}$ ) and  $(\text{UO}_2)_3(\text{OH})_5^+$  ( $474 \pm 7 \text{ mol}^{-1} \text{ cm}^{-1}$ ) respectively in comparison to  $\text{UO}_2^{2+}$  ( $9.7 \pm 0.2 \text{ mol}^{-1} \text{ cm}^{-1}$ ).

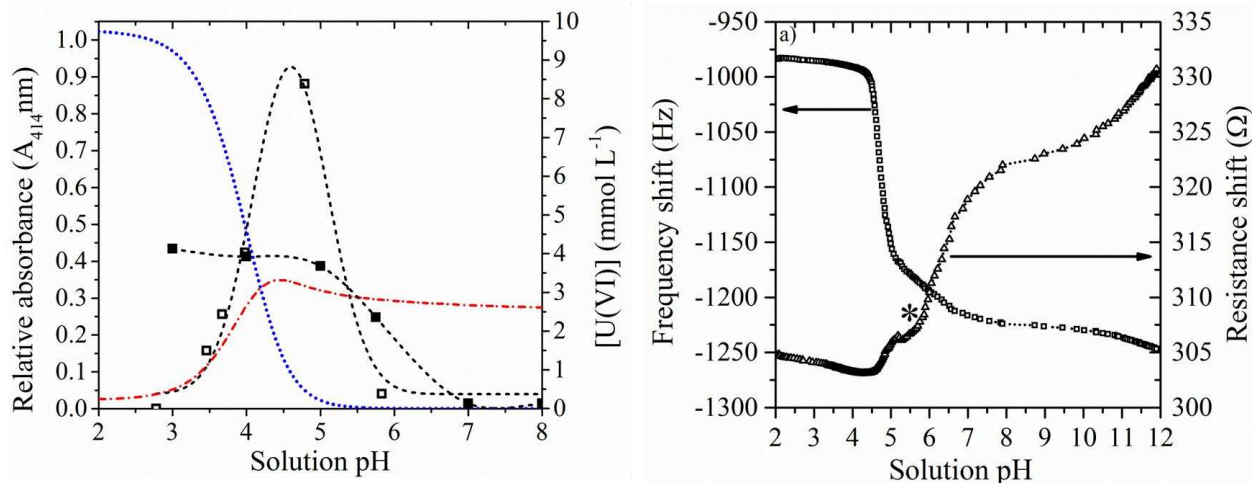


**Figure 1 (a) Solution UV-Vis absorbance at 414nm ( $A_{414}$ ) (black boxes),  $[\text{U(VI)}]$  (black squares), calculated thermodynamic  $\text{UO}_2^{2+}$  (blue dotted line) and total U(VI)-hydroxide species (red dash-dotted line) with respect to pH. (b) QCM  $\Delta F$  and  $\Delta R$  with pH change; \*represents the visible solution cloud point.**

The rapid increase in  $\Delta F$  and  $\Delta R$  (Figure 1b) coincides with U(VI)-hydroxide formation and the expected (Figure 1a – blue dots, red dash-dots) and observed (Figure 1a – black squares) removal of U(VI) from solution beyond pH4.7 ( $A_{414 \text{ max}}$ ). In agreement with the Sauerbrey relationship<sup>20</sup>, where  $\Delta F$  and  $\Delta R$  are proportional to the mass deposited onto the vibrating quartz crystal. I.E. a larger  $\Delta F$  or  $\Delta R$  from equilibrium suggests an increase in particle population in suspension.

Ex-situ DLS analysis of solutions at  $\text{pH} \geq 5$  (Figure 2a) yielded a tri-modal distribution of [143.6-192.7nm], [1751.4-3154.7nm] and [5682.8-10236.4nm] particle populations and a  $d_{50 \text{ volume}} = 5551.7 \text{ nm}$ . Despite this apparent micrometric particle distribution, TEM images (Figure 2a) revealed a relatively monodisperse population of  $14.06 \pm 2.25 \text{ nm}$  nanocrystals with FT-derived d-spacing  $3.1\text{-}3.3 \text{ \AA}$  (-111),  $2.6\text{-}2.7 \text{ \AA}$  (111) and  $1.8\text{-}1.9 \text{ \AA}$  (-311) that correspond to the diffraction peaks for calcium polyuranate ( $\text{Ca}_2\text{U}_3\text{O}_{11}$ ; corroborating with the  $[\text{Ca}/\text{U}]_{\text{ICP-OES}}$  of 0.67).

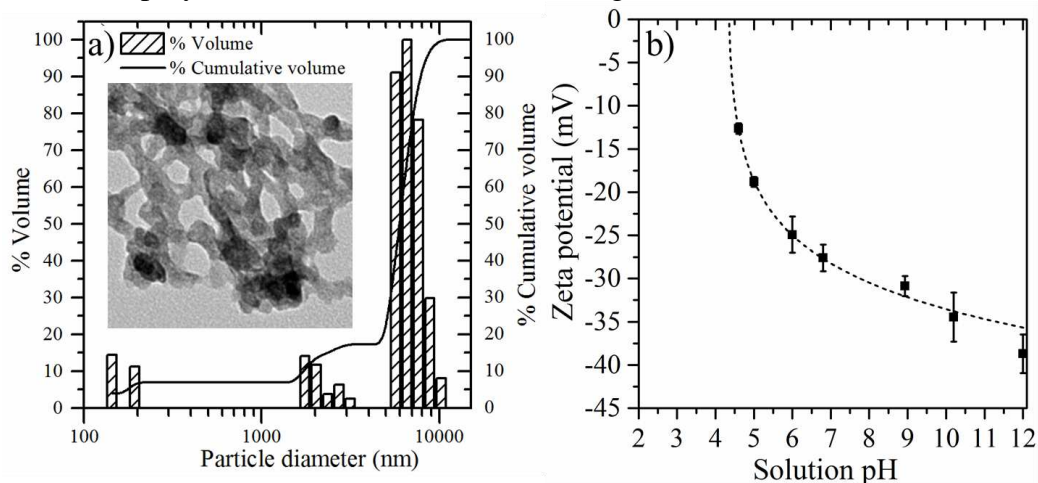


**Figure 2 (a) Particle size distributions at pH5.5 as a function of %volume and TEM image of the particles (image width = 100nm). (b) Zeta potential of Ca<sub>2</sub>U<sub>3</sub>O<sub>11</sub> as a function of pH.**

Given that only solutions above the critical pH5 yielded detectable particles; rapid primary nucleation may occur via solution supersaturation in uranyl hydroxide species at pH4.7 and is therefore, dependent on hydroxide concentration. However, as the isoelectric point of these particles lies at pH4.35 (Figure 2b), immediate aggregation of primary nanocrystals occurs after nucleation due to electric double layer contraction.

The condensation of uranyl hydroxide species forms lamellar uranyl oxo layers stabilized by interstitial Ca<sup>2+</sup>, it is therefore conceivable that primary nucleation pH may be reduced as a function of increasing Ca<sup>2+</sup> concentration. Whilst this exact relationship requires further study, particle Ca<sup>2+</sup> incorporation is possible until [Ca/U] = 1 by tuning precursor solution stoichiometry.

**High temperature curing processes**

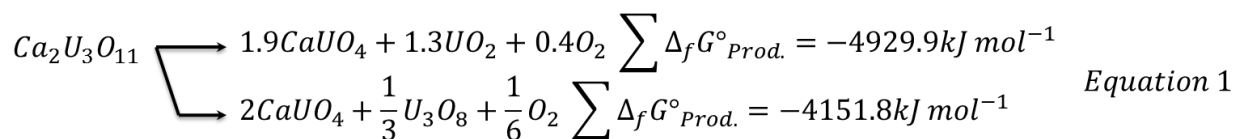
Several physical and visual changes are apparent during thermal curing of the precipitated particles as summarized in Table I.

**Table I Summary of weight loss processes in TGA-DSC analysis (Visual coloration of particles detailed in parentheses)**

Region	Temperature range (°C)	Notes (inferred reaction processes)
1	50-175	6% wt. loss. Hydrate volatilization (orange)
2	175-600	3.5% wt. loss. Dehydroxylation (dark orange)
3a	600-700	Mixed phase formation (dark orange- ochre)
3b	700-800	Phase transformation (ochre- dark green specks)
4	800-950	1% wt. loss Oxygen loss (black- dark green hue)
5	900-1000	Stable plateau (black)

The XRD pattern of orange Ca<sub>2</sub>U<sub>3</sub>O<sub>11</sub> particles (Figure 3b - 25°C) resemble a Ca-bearing endmember of the Ianthanite – Becquerelite - Compreignacite mineral group (Figure 3b diamonds)<sup>21</sup> formed under similar conditions with differing calcium content, suggesting structural isomorphology in the 0.25 ≤ [Ca/U] ≤ 1 range. During curing up to 700°C (Figure 2a), the precipitates decompose to form spherical particles composed of crystalline calcium polyuranate (Ca<sub>2</sub>U<sub>3</sub>O<sub>11</sub>) (Figure 3b – 700°C, circles) via an initial 6wt. % loss of surface water and a secondary 3.5% wt. loss of zeolitic water.

The spherical Ca<sub>2</sub>U<sub>3</sub>O<sub>11</sub> particles (Figure 3) sinter towards spheroidal aggregates by 900°C. This coincides with a color transition towards black, implying chemical reduction from U(VI) to U(IV). This reduction coincides with a 1wt. % loss (0.4mol O<sub>2</sub> per mol Ca<sub>2</sub>U<sub>3</sub>O<sub>11</sub>) (Figure 3a 800-900°C) and is revealed by XRD-Rietveld analysis (Figure 3b 800-1000°C) to occur via conversion to 65.6±3.25wt% CaUO<sub>4</sub> (PDF: 04-007-9392) and 34.4±3.25wt% UO<sub>2</sub> (PDF: 04-008-7779). A similar reduction phenomena is observed in the UO<sub>3</sub> - U<sub>3</sub>O<sub>8</sub> transition at ~600°C under N<sub>2</sub><sup>22</sup>. However taking into account the Δ<sub>f</sub>G° of UO<sub>2</sub> (-1031.8±1.0 kJ mol<sup>-1</sup> <sup>23</sup>), U<sub>3</sub>O<sub>8</sub> (-1123.2±0.8 kJ mol<sup>-1</sup> <sup>23</sup>) and CaUO<sub>4</sub> (-1888.7±2.4 kJ mol<sup>-1</sup> <sup>23</sup>), it is evident that formation of UO<sub>2</sub> is favored thermodynamically compared to U<sub>3</sub>O<sub>8</sub> in the presence of CaUO<sub>4</sub> (Equation 1).



An increase in bulk uranate particle calcium content towards  $[\text{Ca}/\text{U}] = 1$ , phases in the particles yielded by curing tend towards a pure calcium monouranate phase (Figure 3c boxes, insert ii), whereas excess calcium is segregated as  $\text{Ca}(\text{OH})_2$  in the precipitate (data not shown). This excess calcium is sequestered as  $\text{Ca}_3\text{UO}_6$  when cured at  $800^\circ\text{C}$ , resulting in the mixture of  $\text{CaUO}_4$  and  $\text{Ca}_3\text{UO}_6$  (Figure 3c insert i); whilst the latter is still within the uranate family, its crystal structure has changed towards a distorted perovskite, with infinite uranate sheets bound via uranyl oxygens.

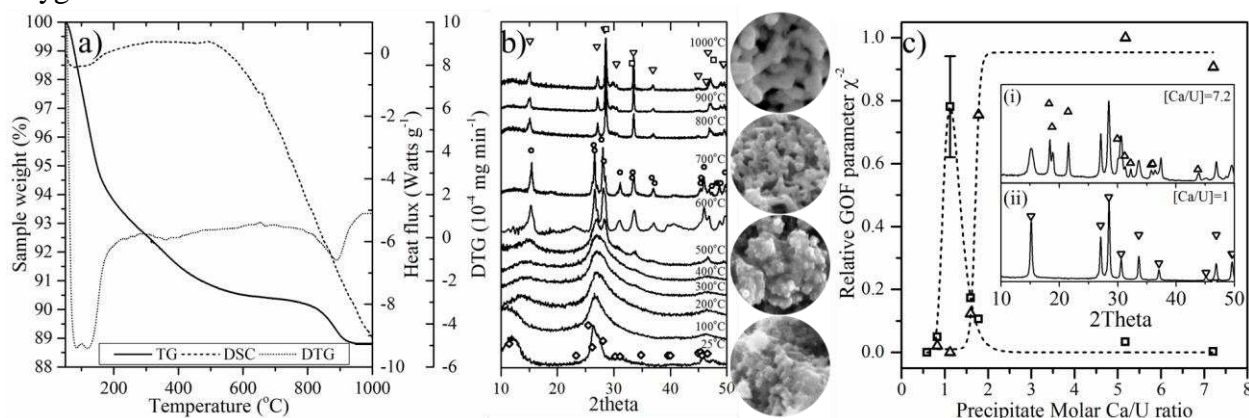


**Figure 3** (a) Sample curing profile in the  $50\text{-}1000^\circ\text{C}$  range at  $10^\circ\text{C}/\text{min}$ . (b) XRD patterns of calcium uranate particles cured between  $25^\circ\text{C}$  -  $1000^\circ\text{C}$  with corresponding secondary electron SEM images (diam. =  $1\mu\text{m}$ ) of  $25$ ,  $300$ ,  $700$  and  $1000^\circ\text{C}$  particles ( $\diamond$   $\text{Ca}_{1.5}(\text{OH})((\text{UO}_2)_6\text{O}_4(\text{OH})_6)\cdot 7\text{H}_2\text{O}$ ;  $\circ$   $\text{Ca}_2\text{U}_3\text{O}_{11}$ ;  $\square$   $\text{UO}_2$ ;  $\nabla$   $\text{CaUO}_4$ ). (c) Relative Rietveld goodness of fit parameter ( $\chi^2$ ) of particle XRD patterns to  $\text{CaUO}_4$  (PDF: 04-007-9392, boxes) and  $\text{Ca}_3\text{UO}_6$  (PDF: 04-009-1244, triangles) as a function of  $[\text{Ca}/\text{U}]$  ratio after curing at  $800^\circ\text{C}$ . Insert: phase segregation into  $\text{CaUO}_4$  ( $\nabla$ ) and  $\text{Ca}_3\text{UO}_6$  ( $\Delta$ ) with (i)  $[\text{Ca}/\text{U}] = 1$  and (ii)  $[\text{Ca}/\text{U}] = 7.2$ .

The uranate particles with  $0.25 \leq [\text{Ca}/\text{U}] \leq 1$  exhibited almost identical XRD patterns up to  $500^\circ\text{C}$  before segregating to  $\text{CaUO}_4$  and  $\text{Ca}_2\text{U}_3\text{O}_{11}$  ( $[\text{Ca}/\text{U}] < 1$ ) or  $\text{CaUO}_4$  and  $\text{Ca}_3\text{UO}_6$  ( $[\text{Ca}/\text{U}] > 1$ ).  $[\text{Ca}/\text{U}] = 1$  is therefore the upper limit of isomorphous calcium incorporation into the uranate structure below at a maximum curing temperature of  $500^\circ\text{C}$ ; further study is being undertaken to understand how calcium migration occurs during curing processes.

## CONCLUSIONS

A simple process for the synthesis of stable calcium monouranate particles as a uranic wasteform or for use in thermodynamic/kinetic studies has been demonstrated via aqueous reaction followed by a short curing step. It was shown that particle formation occurs via rapid nucleation at pH4.7 and that phase purity can be tuned by altering precursor solution  $[\text{Ca}/\text{U}]$  stoichiometry and pH. An isomorphous uranate structural range of stoichiometry has been identified between  $0.25 \leq [\text{Ca}/\text{U}] \leq 1$

and further study is underway to understand how solid state calcium migration occurs in the uranate structure.

## ACKNOWLEDGMENTS

The authors gratefully acknowledge the financial support of the Engineering and Physical Sciences Research Council (EPSRC), Nuclear Decommissioning Authority (NDA) and Sellafield Ltd in this research.

## REFERENCES

1. L. P. Moroni and F. P. Glasser, *Waste Manage* **15** (3), 243-254 (1995).
2. P. Bots, K. Morris, R. Hibberd, G. T. W. Law, J. F. W. Mosselmans, A. P. Brown, J. Douch, A. J. Smith and S. Shaw, *Langmuir* **30** (48), 14396-14405 (2014).
3. R. J. Finch and R. C. Ewing, *Am Mineral* **82** (5-6), 607-619 (1997).
4. N. Mace, E. Wieland, R. Dahn, J. Tits and A. C. Scheinost, *Radiochim Acta* **101** (6), 379-389 (2013).
5. E. H. P. Cordfunke and B. O. Loopstra, *Journal of Inorganic and Nuclear Chemistry* **29** (1), 51-57 (1967).
6. H. R. Hoekstra and J. J. Katz, *J Am Chem Soc* **74** (7), 1683-1690 (1952).
7. W. H. Zachariasen, *Acta Crystallographica* **1** (1-6), 281-285 (1948).
8. B. O. Loopstra and H. M. Rietveld, *Acta Crystallographica Section B* **25** (4), 787-791 (1969).
9. H. Rietveld, *Acta Crystallographica* **20** (4), 508-513 (1966).
10. A. K. Gupta and M. Gupta, *Biomaterials* **26** (18), 3995-4021 (2005).
11. S. Laurent, D. Forge, M. Port, A. Roch, C. Robic, L. Vander Elst and R. N. Muller, *Chemical Reviews* **108** (6), 2064-2110 (2008).
12. J. Janov, P. G. Alfredson and V. K. Vilkaitis, *Journal of Nuclear Materials* **44** (2), 161-174 (1972).
13. R. A. Reibold, J. F. Poco, T. F. Baumann, R. L. Simpson and J. H. Satcher Jr, *Journal of Non-Crystalline Solids* **319** (3), 241-246 (2003).
14. M. C. Ball, C. R. G. Birkett, D. S. Brown and M. J. Jaycock, *Journal of Inorganic and Nuclear Chemistry* **36** (7), 1527-1529 (1974).
15. T. R. Griffiths and V. A. Volkovich, *Journal of Nuclear Materials* **274** (3), 229-251 (1999).
16. C. Tanford, R. L. Tichenor and H. A. Young, *J Am Chem Soc* **73** (9), 4491-4492 (1951).
17. E. Giffaut, M. Grivé, P. Blanc, P. Vieillard, E. Colàs, H. Gailhanou, S. Gaboreau, N. Marty, B. Madé and L. Duro, *Appl Geochem* **49**, 225-236 (2014).
18. R. Guillaumont and F. J. Mompean, (2003).
19. G. Meinrath, *J Radioanal Nucl Ch* **224** (1-2), 119-126 (1997).
20. G. Sauerbrey, *Zeitschrift für Physik* **155** (2), 206-222 (1959).
21. J. Skakle, L. Moroni and F. Glasser, *Powder Diffraction* **12** (02), 81-86 (1997).
22. V. J. Wheeler, R. M. Dell and E. Wait, *Journal of Inorganic and Nuclear Chemistry* **26** (11), 1829-1845 (1964).
23. I. Grenthe, H. Wanner and I. Forest, (1992).